AGU PUBLICATIONS

Geophysical Research Letters

RESEARCH LETTER
10.1002/2015GL065973

Key Points:
- Double ITCZ bias persists from CMIP3 to CMIP5
- The CMIP5 MME with overall warmer SST suffers a more serious double ITCZ problem than CMIP3 MME
- No improvement can be identified in the subensembles of five best models from CMIP3 to CMIP5

Correspondence to:
M. Zhang,
Minghua.zhang@stonybrook.edu

Citation:
Zhang, X., H. Liu, and M. Zhang (2015), Double ITCZ in Coupled Ocean-Atmosphere Models: From CMIP3 to CMIP5, *Geophys. Res. Lett.*, *42*, 8651–8659, doi:10.1002/2015GL065973.

Received 31 AUG 2015
Accepted 5 OCT 2015
Accepted article online 8 OCT 2015
Published online 29 OCT 2015

Double ITCZ in Coupled Ocean-Atmosphere Models: From CMIP3 to CMIP5

Xiaoxiao Zhang[1,2], Hailong Liu[1], and Minghua Zhang[3]

[1]State Key Laboratory of Numerical Modeling for Atmospheric Sciences and Geophysical Fluid Dynamics, Institute of Atmospheric Physics, Chinese Academy of Sciences, Beijing, China, [2]College of Earth Science, University of Chinese Academy of Sciences, Beijing, China, [3]School of Marine and Atmospheric Sciences, Stony Brook University, Stony Brook, New York, USA

Abstract Recent progress in reducing the double Intertropical Convergence Zone bias in coupled climate models is examined based on multimodel ensembles of historical climate simulations from Phase 3 and Phase 5 of the Coupled Model Intercomparison Project (CMIP3 and CMIP5). Biases common to CMIP3 and CMIP5 models include spurious precipitation maximum in the southeastern Pacific, warmer sea surface temperature (SST), weaker easterly, and stronger meridional wind divergences away from the equator relative to observations. It is found that there is virtually no improvement in all these measures from the CMIP3 ensemble to the CMIP5 ensemble models. The five best models in the two ensembles as measured by the spatial correlations are also assessed. No progress can be identified in the subensembles of the five best models from CMIP3 to CMIP5 even though more models participated in CMIP5; the biases of excessive precipitation and overestimated SST in southeastern Pacific are even worse in the CMIP5 models.

1. Introduction

Coupled ocean-atmospheric climate models tend to simulate a double Intertropical Convergence Zone (ITCZ) that is characterized by two zonal bands of annual precipitation in the equatorial central Pacific that is not present in observations [e.g., *Mechoso et al*., 1995; *Lin*, 2007]. The spurious double ITCZ not only creates biases of latent heating in the tropics that can impact midlatitude weather and climate through atmospheric teleconnections [*Schneider et al*., 2009; *Manganello and Huang*, 2009] but also affects the intensity of the Hadley circulation and the distribution of the trade winds that are directly related with the simulation of El Niño events.

Ever since this phenomenon was systematically documented by *Mechoso et al*. [1995], many studies have attempted to eliminate this bias in these models [e.g., *Schneider*, 2002; *Dai et al*., 2005; *Zhang and Wang*, 2006; *Song and Zhang*, 2009; *Yu et al*., 2013]. These studies often target individual models at different stages of their developments that have very different sophistications in their physical parameterizations. The objective of this paper is to examine the collective progress of climate models in reducing the double ITCZ from the time of Coupled Model Intercomparison Project Phase 3 (CMIP3) [*Meehl et al*., 2007] to Phase 5 (CMIP5) [*Taylor et al*., 2009]. The results are intended to provide guidance to future improvements of models. They can also serve as benchmarks to measure future models. In addition to assessing the ensembles of models, we also compare the best performing models that participated in CMIP3 and CMIP5, respectively.

2. Data and Models

We used the following observations to evaluate the models. For the precipitation, we use the monthly mean precipitation data from the Global Precipitation Climatology Project (GPCP) [*Adler et al*., 2003] during 1979–2005 gridded at 2.5°×2.5° grid. The monthly mean sea surface temperature (SST) data are obtained from the Hadley Centre SST (Hadley Centre Sea Ice and Sea Surface Temperature (HadISST)) [*Rayner et al*., 2003] with a resolution of 1°×1°. The monthly surface winds are taken from the European Center for Medium-Range Weather Forecasts Re-Analysis (ERA-40) [*Uppala et al*., 2005].

The output from the 20th century simulations (20C3M) of 23 CMIP3 models and the historical runs of 47 CMIP5 models available at the Program for Climate Model Diagnosis and Intercomparison (PCMDI) [http://www-pcmdi.llnl.gov] are used in this paper. If there are more than one runs, only one ensemble member, r1i1p1, is selected. All the data described above are interpolated onto a regular 1°×1° longitude-latitude grid

Table 1a. A Brief Description of CMIP3 and CMIP5 Models Used in This Study

CMIP I.D. (Label in Figures)	Atmospheric Resolution (Lon × Lat)	Oceanic Resolution (Lon × Lat)	Originating Group(s), Country
bccr_bcm2_0	2.81°×2.81°	1.5°×0.5°~1.5°	Bjerknes Centre for Climate Research, Norway
cgcm3_1_t47	3.75°×3.75°	1.9 °×1.9°	Canadian Centre for Climate Modelling and Analysis (CCCMA), Canada
cgcm3_1_t63	2.81°×2.81°	1.4°×0.9°	CCCMA, Canada
cnrm_cm3	2.81°×2.81°	2°×0.5°~2°	Centre National de Recherches Meteorologiques (CNRM), France
csiro_mk3_0	1.875°×1.875°	1.9°×0.8°	Commonwealth Scientific and Industrial Research Organisation (CSIRO), Australia
csiro_mk3_5	1.875°×1.875°	1.9°×0.8°	CSIRO, Australia
gfdl_cm2_0	2.5°×2°	1°×0.3°~1°	NOAA Geophysical Fluid Dynamics Laboratory (GFDL), USA
gfdl_cm2_1	2.5°×2°	1°×0.3°~1°	NOAA GFDL, USA
giss_aom	4°×3°	4°×3°	NASA/ Goddard Institute for Space Studies (GISS), USA
giss_model_e_h	5°×4°	2°×2°	NASA/GISS, USA
giss_model_e_r	5°×4°	5°×4°	NASA/GISS, USA
iap_fgoals1_0_g	2.81°×3°	1°×1°	Laboratory of Numerical Modeling for Atmospheric Sciences and Geophysical Fluid Dynamics (LASG), Institute of Atmospheric Physics (IAP), Chinese. Academy of Sciences (CAS), China
ingv_echam4	1.125°×1.125°	2°×2°	Istituto Nazionale Geofisica e Vulcanologia, Italy
inmcm3_0	5°×4°	2.5°×2°	Institute for Numerical Mathematics (INM), Russia
ipsl_cm4	3.75°×2.5°	2°×2°	Institut Pierre-Simon Laplace (IPSL), France
miroc3_2_hires	1.125°×1.125°	0.3°×0.2°	Center for Climate System and Research (CCSR), National Institute for Environmental Studies (NIES), Japan Agency for Marine-Earth Science and Technology (JAMSTEC), Japan
miroc3_2_medres	2.81°×2.81°	1.4°×0.5°~1.4°	CCSR, NIES, JAMSTEC, Japan
mpi_echam5	1.875°×1.875°	1.5 °×1.5°	Max Planck Institute for Meteorology (MPI-M), Germany
mri_cgcm2_3_2a	2.81°×2.81°	2.5°×0.5°~2°	Meteorological Research Institute (MRI), Japan
ncar_ccsm3_0	1.41°×1.41°	1°×0.3°~1°	National Center for Atmospheric Research (NCAR), USA
ncar_pcm1	2.81°×2.81°	1.1°×0.5°~0.7°	NCAR, USA
ukmo_hadcm3	3.75°×2.466°	1.25°×1.25°	Met Office Hadley Centre (MOHC), UK
ukmo_hadgem1	1.875°×1.241°	1°×0.3°~1°	MOHC, UK

by using bilinear interpolation. Model data after calendar year 1979 are used. Several modeling groups conducted simulations with different versions of their models. They are considered as separate models in this study. Table 1a lists the acronyms, resolutions, and the main references of the models in CMIP3. Those for CMIP5 are listed in Table 1b.

3. Results

3.1. Ensemble Mean

Double ITCZ in coupled models has been shown to most clearly appear in the boreal spring season when the sea surface temperature (SST) in the southeastern equatorial Pacific reaches maximum after the southern summer [*Szoeke and Xie*, 2008]. In this season, observed precipitation is also maximum [*Zhang*, 2001]. Figures 1a and 1b show the mean distribution of observed climatological SST and precipitation in March. This month is selected because even in observations there is double ITCZ and as will be shown later this feature is greatly amplified in the models. The solid rectangular box in Figure 1a denotes the area where the biases are calculated (2.5°S–12.5°S, 140°W–90°W). The surface winds are shown in Figures 1c and 1d as northeasterly and southeasterly trade winds over the equatorial Pacific. The transition from positive to negative values of the meridional wind occurs at the latitude of 7°N where the primary ITCZ is located.

The corresponding ensemble averages of the simulated SST, precipitation, and surface winds in CMIP3 models are shown in Figures 1e–1h. Compared with observations, the simulation has a greater region south of the equator, with SST warmer at 27°C and a colder tongue at the equator with temperature up to 2°C lower than observations. This SST distribution accompanies a zonal band of precipitation highlighted in the solid box that is much stronger than observations as shown in Figure 1f. Contrary to the observations, this band of precipitation is also stronger than the one north of the equator, leading to an interhemispheric asymmetric bias.

Errors in the surface winds are the weaker easterly south of the equator and spurious meridional winds diverging away from the equator (Figures 1g and 1h). The maximum values of errors in the surface winds are located just in the solid boxed region. The weaker easterly can be explained by the weaker southeasterly trade winds

Table 1b. A Brief Description of CMIP3 and CMIP5 Models Used in This Study

CMIP I.D. (Label in Figures)	Atmospheric Resolution (Lon × Lat)	Oceanic Resolution (Lon × Lat)	Originating Group(s), Country
ACCESS1-0	1.875°×1.241 °	1°×0.6°	CSIRO- Bureau of Meteorology (BOM), Australia
ACCESS1-3	1.875°×1.268°	1°×0.6°	CSIRO-BOM, Australia
BCC-CSM1-1	2.81°×2.81°	1°×0.78°	Beijing Climate Center (BCC), China Meteorological Administration (CMA), China
BCC-CSM1-1-M	1.125°×1.125°	1°×0.78°	BCC, CMA, China
BNU-ESM	2.81°×2.81°	1°×0.9°	Global Change and Earth System Science, Beijing Normal University BNU, China
CanCM4	2.81°×2.81°	2.3°×0.94°	Canadian Centre for Climate Modelling and Analysis (CCCMA), Canada
CanESM2	2.81°×2.81°	2.3°×0.94°	CCCMA, Canada
CCSM4	1.25°×0.9375°	1.125°×0.47°	NCAR, USA
CESM1-BGC	1.25°×0.9375°	1.125°×0.47°	National Science Foundation (NSF)/DOE NCAR, USA
CESM1-CAM5	1.25°×0.9375°	1.125°×0.47°	NSF/DOE NCAR, USA
CESM1-FASTCHEM	1.25°×0.9375°	1.125°×0.47°	NSF/DOE NCAR, USA
CESM1-WACCM	2.5°×1.875°	2.5°×1.875°	NSF/DOE NCAR, USA
CMCC-CESM	3.75°×3.75°	1.125°×0.47°	Centro EuroMediterraneo sui Cambiamenti Climatici (CMCC), Italy
CMCC-CMS	1.875°×1.875°	1.98°×1.21°	CMCC, Italy
CNRM-CM5	1.406°×1.406°	1°×0.62°	CNRM, Centre Européen de Recherche et de Formation Avancée en Calcul Scientifique (CERFACS), France
CNRM-CM5-2	1.406°×1.406°	1°×0.62°	CNRM, CERFACS, France
CSIRO-Mk3-6-0	1.875°×1.875°	1.875°×0.9375°	CSIRO- Queensland Climate Change Centre of Excellence, Australia
FGOALS-g2	2.81°×3°	1°×1°	LASG, IAP, CAS, China
FGOALS-s2	2.81°×1.67°	1°×1°	LASG, IAP, CAS, China
FIO-ESM	2.81°×2.81°	0.9375°×0.56°	First Institute of Oceanography (FIO), China
GFDL-CM2-1	2.5°×2°	1°×0.9°	NOAA GFDL, USA
GFDL-CM3	2.5°×2°	1°×0.9°	NOAA GFDL, USA
GFDL-ESM2G	2.5°×2°	1°×0.86°	NOAA GFDL, USA
GFDL-ESM2M	2.5°×2°	1°×0.86°	NOAA GFDL, USA
GISS-E2-H	2.5°×2°	1°×1°	NASA/GISS, USA
GISS-E2-H-CC	2.5°×2°	1°×1°	NASA/GISS, USA
GISS-E2-R	2.5°×2°	1.25°×1°	NASA/GISS, USA
GISS-E2-R-CC	2.5°×2°	1.25°×1°	NASA/GISS, USA
HadCM3	3.75°×2.466°	1.25°×1.25°	MOHC, UK
HadGEM2-CC	1.875°×1.241°	1°×0.83 °	MOHC, UK
HadGEM2-ES	1.875°×1.241°	1°×0.83 °	MOHC, UK
HadGEM2-AO	1.875°×1.241 °	1.875°×1.24 °	National Institute of Meteorological Research, South Korea
INMCM4	2°×1.5°	2°×1.5°	INM, Russia
IPSL-CM5A-LR	3.75°×1.875°	3.75°×1.89 °	IPSL, France
IPSL-CM5A-MR	2.5°×1.259°	2.5°×1.26°	IPSL, France
IPSL-CM5B-LR	3.75°×1.895°	3.75°×1.89 °	IPSL, France
MIROC4h	0.56°×0.56°	0.56°×0.56°	Atmosphere and Ocean Research Institute (AORI), NIES, JAMSTEC, Japan
MIROC5	1.41°×1.41°	1.41°×1.41°	AORI, NIES, JAMSTEC, Japan
MIROC-ESM	2.81°×2.81°	1.41°×0.9375°	JAMSTEC/AORI/NIES, Japan
MIROC-ESM-CHEM	2.81°×2.81°	1.41°×0.9375°	JAMSTEC/AORI/NIES, Japan
MPI-ESM-LR	1.875°×1.875°	1.875°×1.875°	MPI-M, Germany
MPI-ESM-MR	1.875°×1.875°	1.875°×1.875°	MPI-M, Germany
MPI-ESM-P	1.837°×1.837°	1.84°×1.84°	MPI-M, Germany
MRI-CGCM3	1.125°×1.125°	1.125°×1.125°	MRI, Japan
MRI-ESM1	1.125°×1.125°	1.125°×1.125°	MRI, Japan
NorESM1-M	2.5°×1.875°	2.5°×1.875°	Norwegian Climate Centre (NCC), Norway
NorESM1-ME	2.5°×1.875°	2.5°×1.875°	NCC, Norway

that terminate before reaching the equator, while bias in the meridional wind can be explained by the anomalous cross-equatorial northerly winds converging toward the biased precipitation south of the equator.

The CMIP5 ensemble mean simulations of the above variables are shown in the last column of Figure 1. It is seen that the biases described for CMIP3 models also exist in CMIP5 models: (1) warm SST bias in the eastern equatorial Pacific south of the equator, (2) colder tongue at the equator, (3) wrong asymmetry of precipitation between the northern and southern hemispheres relative to the equator, (4) weaker easterly south of the equator, and (5) spurious meridional wind divergence away from the equator.

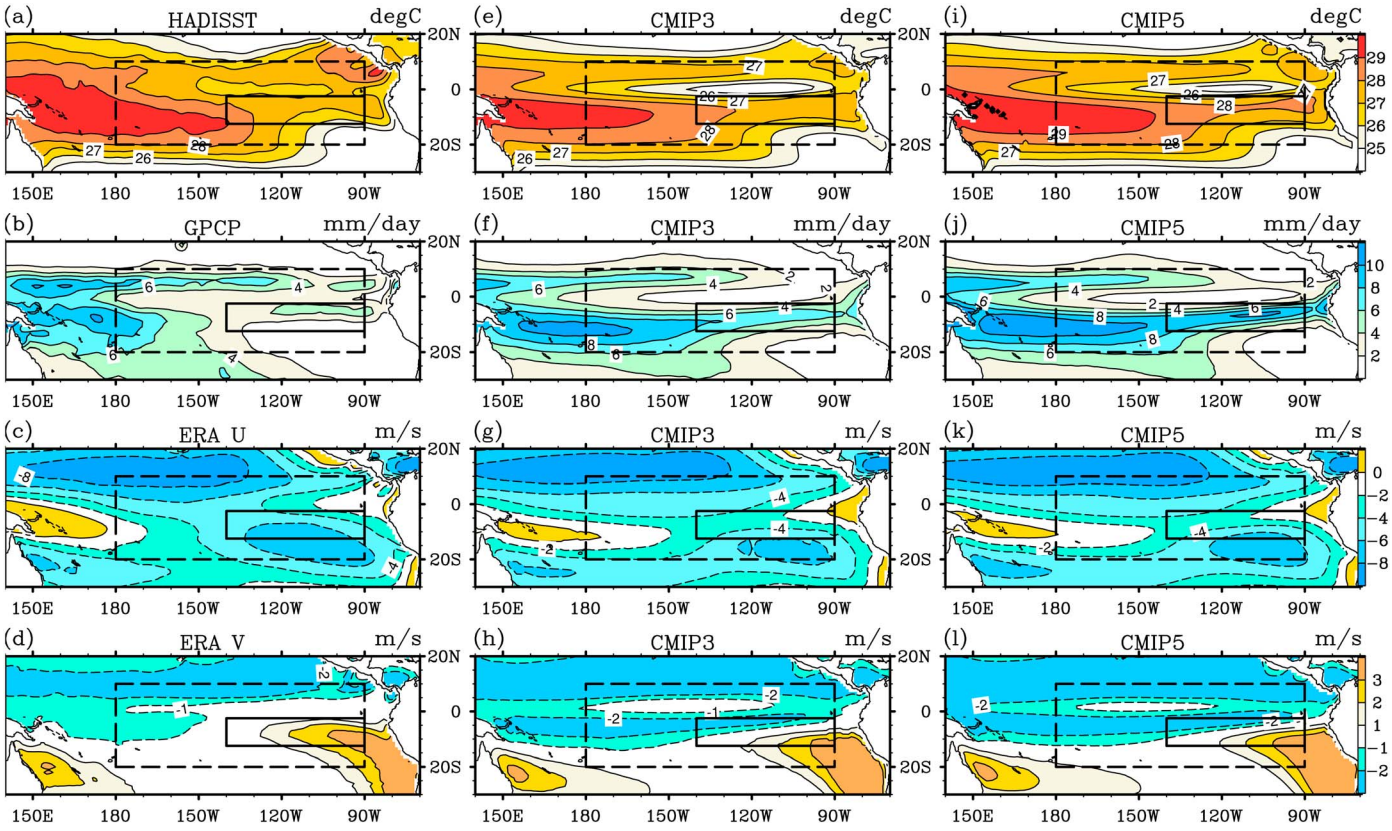

Figure 1. (a) Sea surface temperature from HadISST during 1979–2005 (°C), (b) precipitation from GPCP during 1979–2005 (mm/d), (c) zonal, and (d) meridional wind at 10 m from ERA-40 during 1979–2005 (m/s) for March. (e–l) Same as Figures 1a–1d but for multimodel ensemble means for CMIP3 and CMIP5, respectively.

To examine the performance difference between the CMIP3 and CMIP5 ensembles, we show in Figure 2 the biases of model simulations against observations for the month of March and for the annual averages. In March (Figures 2a–2d), SST (Figures 2a and 2b) in CMIP5 is overall warmer than in CMIP3. This exacerbates the warm bias in the southeastern Pacific, including the bias off the Peru coasts. The warm SST in CMIP5 leads to a greater double ITCZ bias in precipitation (Figures 2c and 2d) than in CMIP3 models.

In the Figures 2e–2h, we show the annually averaged biases. It is seen that the SST biases are similar to those in March (Figures 2e and 2f). The differences between the two annual ensembles are also similar to those in March. The double ITCZ and the cold bias along the equator are smaller than those in March (Figures 2g and 2h). This reflects the fact that the double ITCZ reaches maximum in northern spring as mentioned earlier. The CMIP5 double ITCZ bias in annual precipitation is also worse than that in CMIP3 models.

3.2. Ensemble Distribution

The performance distribution of individual models in the two ensembles is next examined by using pattern correlation and simulation biases. The pattern correlation is calculated in the domain of 20°S–10°N,180°–90°W donated by the dotted line box in Figure 1a, and the biases of precipitation and SST are calculated in the region of 2.5°S–12.5°S,140°W–90°W denoted by the solid line box in Figure 1a. Only results from March are presented. Figures 3a and 3b show the distributions of the correlation coefficients for precipitation arranged in ascending order. The names of the models are listed in Tables 1a and 1b. The same modeling groups appear in the same color and the ensemble mean correlations are shown by the red line.

The models simulated a wide range of correlations in both ensembles. The range in the CMIP3 models is from −0.05 to 0.81; in CMIP5 it is 0.09 to 0.78. It appears that the worst CMIP3 models in this measure have been improved. The ensemble correlation in CMIP5 models is almost the same as in CMIP3 (0.56). Differences can be found only in the third digit after floating. The biases in precipitation are shown in Figure 3c for CMIP3 models and Figure 3d for CMIP5 models. Most models overestimate precipitation except two CMIP3 models

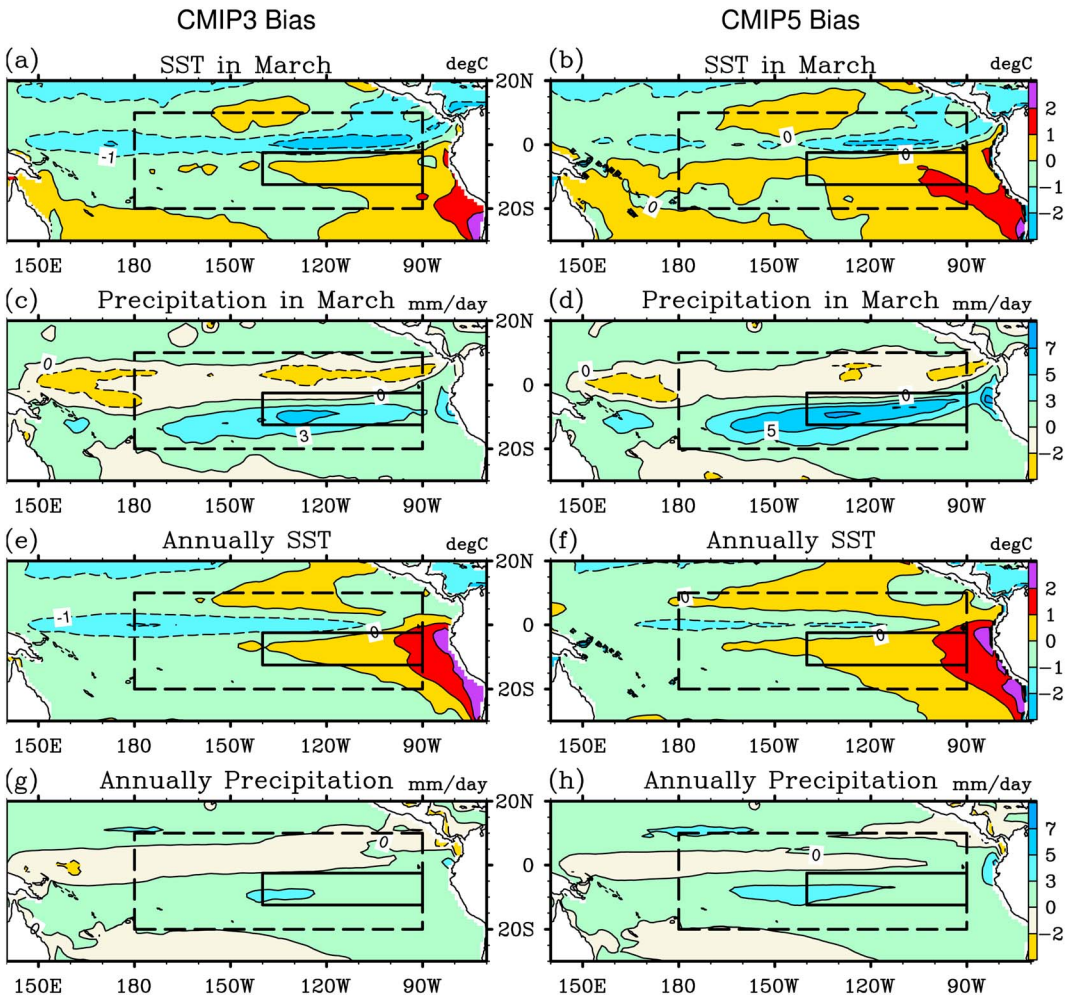

Figure 2. (a–d) Biases of model simulations against the observations for March. (Figures 2a and 2b) Biases in SST (°C) for CMIP3 and CMIP5. (Figures 2c and 2d) Same as Figures 2a and 2b but for the precipitation (mm/d). (e–h) Same as Figures 2a–2d but for the annual mean.

(mri_cgcm2.3.2a, ukmo_hadcm3) and one CMIP5 model (HadCM3). Twenty-five percent of the CMIP3 models and 55% of the CMIP5 models have biases larger than 4.0 mm/d, which leads to a marked increase of the ensemble mean bias from 2.8 mm/d in CMIP3 to 4.0 mm/d in CMIP5 models.

Figures 3e and 3f show the distribution of SST biases in CMIP3 and CMIP5, respectively. The models are arranged in the same order as in Figures 3c and 3d for precipitation. The range for CMIP3 is from −1.1°C to 1.6°C, while it is −1.3°C to 2.5°C for CMIP5, about 1°C wilder than CMIP3. The ensemble mean SST bias for CMIP5 is 0.58°C, about 0.43°C higher than that in CMIP3. There is evidence of positive correlation between the SST biases and the precipitation biases among the models, especially in the CMIP5 models.

In summary, neither the ensemble means nor the discrepancy among the models has been improved from CMIP3 to CMIP5. CMIP5 models as a whole perform even a little worse than CMIP3 models in the bias measures. We also examined the possible dependence of the double ITCZ bias on the model resolution. No relationship is found from the resolutions given in Tables 1a and 1b.

3.3. The Subensemble of the Best Five Models

From CMIP3 to CMIP5, some modeling groups have upgraded their models significantly such as the Community Climate System Model [*Gent et al.*, 2011]; others may have made little changes to their models. We therefore constructed a subensemble of the five best models in CMIP3 and CMIP5 models to see whether the performances of the top models have been improved from CMIP3, bearing in mind that CMIP5 has about

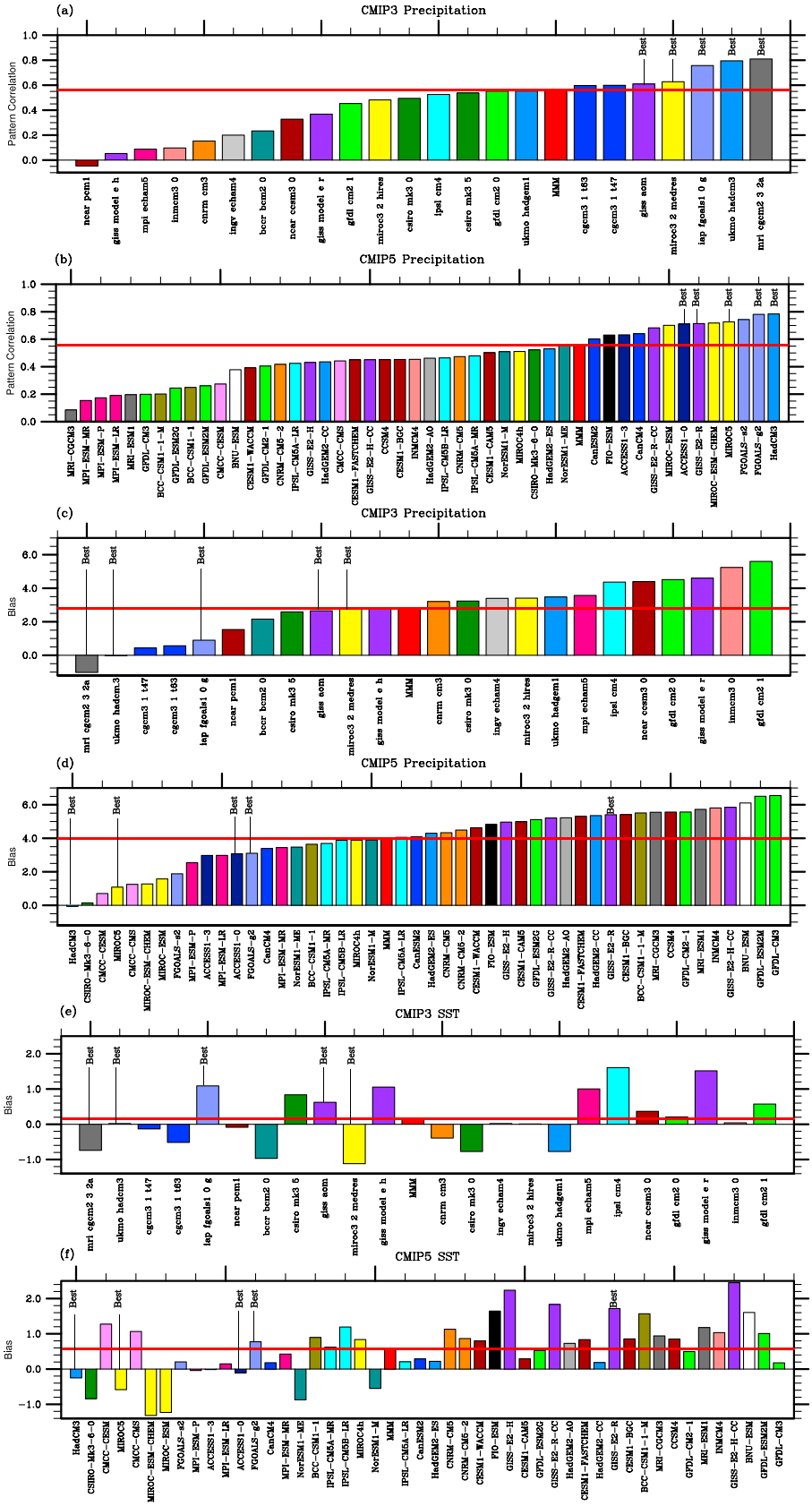
(a)
CMIP3 Precipitation
Pattern Correlation
(b)
CMIP5 Precipitation
Pattern Correlation
(c)
CMIP3 Precipitation
Bias
(d)
CMIP5 Precipitation
Bias
(e)
CMIP3 SST
Bias
(f)
CMIP5 SST
Bias
Best

Figure 3

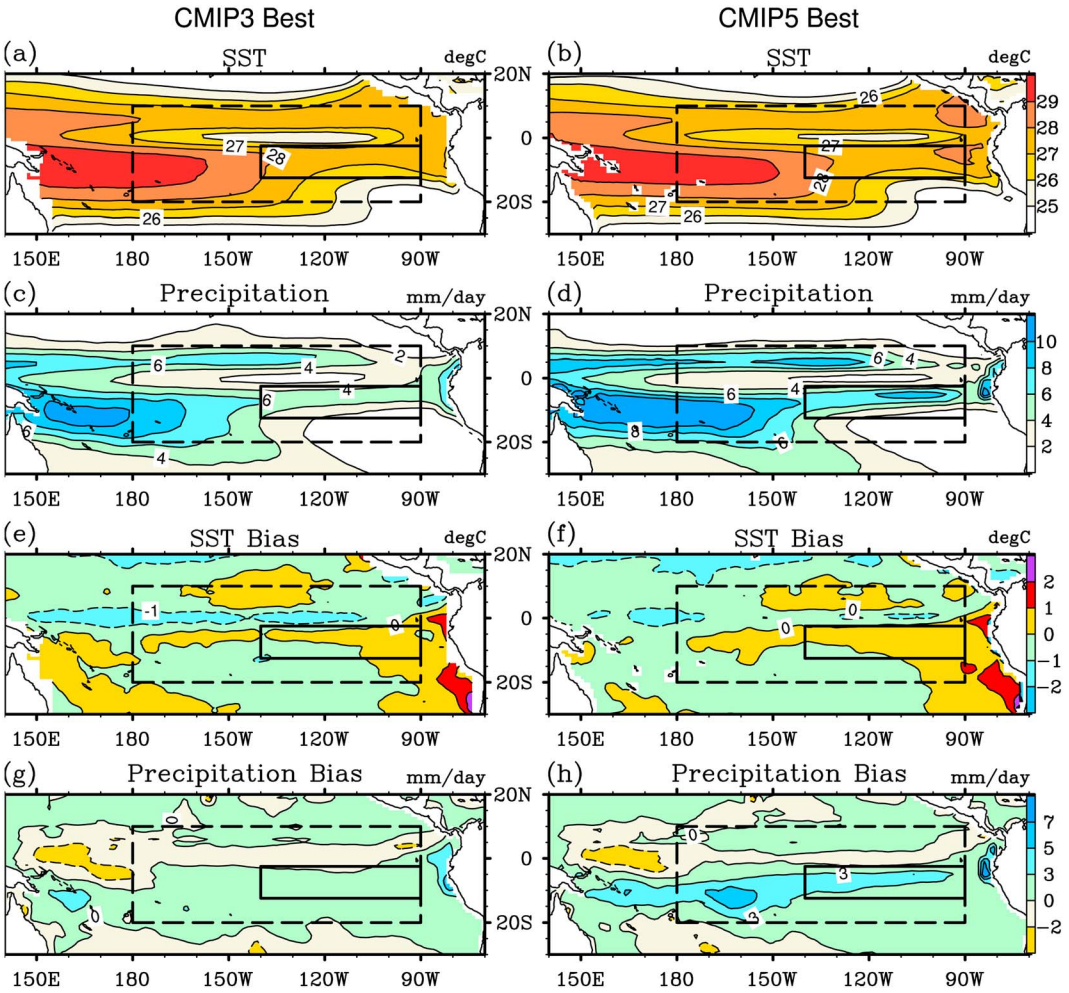

Figure 4. Five best model ensemble mean SST (°C) for (a) CMIP3 and (b) CMIP5 during March. (c and d) Same as Figures 4a and 4b but for precipitation (mm/d). (e–h) Same as Figures 4a–4d but for the biases against the observation.

twice as many models as CMIP3 does. The selection of the best models is based on the simple measure of pattern correlation of precipitation in the domain of 20°S–10°N,180°–90°W for March. We note that the best correlation may not reflect the best performances of the models in other metrics. More elaborate metrics may be designed such as the Taylor diagram [*Taylor*, 2001] or empirical orthogonal function modes as by *Li et al.* [2015]. It is adopted here because of its simplicity and intuitive interpretation. Since the performances of different model versions from the same modeling groups tend to cluster together, we selected the five models from different modeling centers, each as the best performing version if multiple versions exist. The best subensemble in CMIP3 includes ukmo_hadcm3, iap_fgoals1_0_g, miroc3_2_medres, giss_aom, and mri_cgcm2_3_2a; the subensemble in CMIP5 includes HadCM3, FGOALS-g2, MIROC5, GISS-E2-R, and ACCESS1-0. The dry band on the equator is absent in FGOALS-g2 and GISS-E2-R and the excessive precipitation in the southeast Pacific is absent in mri_cgcm2_3_2a, iap_fgoals1_0, ukmo_hadcm3, and GISS-E2-R (not shown).

The comparison of simulation results between the two best ensembles is given in Figure 4. The top two rows show the mean SST and precipitation respectively, while the bottom two rows show the biases relative to

Figure 3. The spatial correlation coefficients of the precipitation between model and the observation over the domain of 20°S–10°N,180°–90°W arranged in ascending order of their magnitudes for (a) CMIP3 and (b) CMIP5. (c and d) Same as Figures 3a and 3b but for the model biases in the precipitation (mm/d) over the domain of 2.5°S–12.5°S,140°W–90°W. (e and f) Same as Figures 3c and 3d but for the model biases in SST (°C) arranged in the same order of Figures 3c and 3d.

observations. The left column is for CMIP3 while the right column is for CMIP5. The warm and wet biases in highlighted area of the southeastern Pacific are significantly smaller in the five best models than in the total ensembles. Nevertheless, the dry and cold biases at the equator and the wet and warm biases in the southeast equatorial Pacific are still evident. We also cannot find improvement from CMIP3 to CMIP5 in the top models, especially in the southeast equatorial Pacific. The warm and wet biases in the highlighted region for CMIP5 are in fact larger than for CMIP3 models.

4. Summary

We examined the performances of the CMIP3 and CMIP5 models in simulating SST, precipitation, and surface winds in the equatorial pacific. Both ensembles of models are found to simulate the spurious rainband, warm SST, weak trade winds, and strong meridional wind divergence in the southeast equatorial Pacific. Compared with CMIP3 models, there is no evidence of improvements in both the precipitation and the SST by the CMIP5 models. The double ITCZ biases are also in the top ensemble of the five best models as measured by pattern correlations, with results from CMIP5 somewhat worse than those from CMIP3, especially in the precipitation.

The lack of progress in reducing the double ITCZ bias from CMIP3 to CMIP5 is likely due to several known model biases that have persisted through generations of coupled models. These include the inadequate simulations of stratocumulus clouds in the southeastern Pacific and the stratocumulus to cumulus transition away from the coast, the triggering and entrainment parameterizations of deep convection, insufficient resolution of the models in resolving mesoscale eddy transport in the ocean, and the upwelling along the coast [*Mechoso et al*., 2014]. It calls for the need to better understand the physical causes of the double ITCZ bias in coupled climate models. Several studies in recent years have revealed possible causes of this bias. For example, models with more energy flux into the southern hemisphere ocean tend to have a stronger double ITCZ bias, which is closely related to the cloud biases over the Southern Ocean [*Hwang and Frierson*, 2013; *Li and Xie*, 2014]. Deep convection with more realistic representation of the humidity dependence of entrainment has been suggested to impact this bias [*Hirota et al*., 2011; *Hirota and Takayabu*, 2012]. These process level understandings, however, are yet to be translated to better model performances. It is hoped that results from this paper will lead to more attentions to the double ITCZ problem that will motivate future research to eliminate this bias.

Acknowledgments

We wish to thank the two anonymous reviewers whose comments have helped us to improve the paper. We thank all the modeling groups, the PCMDI and the World Climate Research Programme's Working Group on Coupled Modeling for their efforts in making available the CMIP multimodel data sets. All data used in this paper are available upon request from the first author (xiaoxiao_zhang@mail.iap.ac.cn). This research is supported by the Strategic Priority Research Program entitled "Western Pacific Ocean System: Structure, Dynamics and Consequences" of the Chinese Academy of Sciences (grant XDA11010304) and the Major National Basic Research Program of China (973 Program) on Global Change under grant 2010CB951800, by the Biological and Environmental Research Division in the Office of Sciences of the U.S. Department of Energy (DOE) and the National Science Foundation to the Stony Brook University.

References

Adler, R. F., et al. (2003), The version 2 Global Precipitation Climatology Project (GPCP) monthly precipitation analysis (1979-Present), *J. Hydrometeorol.*, *4*, 1147–1167, doi:10.1175/1525-7541(2003)004<1147:TVGPCP>2.0.CO;2.

Dai, F., R. Yu, X. Zhang, Y. Yu, and J. Li (2005), Impacts of an improved low-level cloud scheme on the eastern Pacific ITCZ-cold tongue complex, *Adv. Atmos. Sci.*, *22*(4), 559–574, doi:10.1007/BF02918488.

Gent, P. R., et al. (2011), The Community Climate System Model Version 4, *J. Clim.*, *24*(19), 4973–4991, doi:10.1175/2011JCLI4083.1.

Hirota, N., and Y. N. Takayabu (2012), Reproducibility of precipitation distribution over the tropical oceans in CMIP5 multiclimate models compared to CMIP3, *Clim. Dyn.*, *41*, 2909–2920, doi:10.1007/s00382-013-1839-0.

Hirota, N., Y. N. Takayabu, M. Watanabe, and M. Kimoto (2011), Precipitation reproducibility over tropical oceans and its relationship to the double ITCZ problem in CMIP3 and MIROC5 climate models, *J. Clim.*, *24*(18), 4859–4873, doi:10.1175/2011JCLI4156.1.

Hwang, Y. T., and D. M. W. Frierson (2013), Link between the double-Intertropical Convergence Zone problem and cloud biases over the Southern Ocean, *Proc. Natl. Acad. Sci. U.S.A.*, *110*(13), 4935–4940, doi:10.1073/pnas.1213302110.

Li, G., and S. P. Xie (2014), Tropical biases in CMIP5 multimodel ensemble: The excessive equatorial pacific cold tongue and double ITCZ problems, *J. Clim.*, *27*(4), 1765–1780, doi:10.1175/JCLI-D-13-00337.1.

Li, G., Y. Du, H. M. Xu, and B. H. Ren (2015), An intermodel approach to identify the source of excessive equatorial pacific cold tongue in CMIP5 models and uncertainty in observational data sets, *J. Clim.*, *28*, 7630–7640, doi:10.1175/JCLI-D-15-0168.1.

Lin, J.-L. (2007), The double-ITCZ problem in IPCC AR4 coupled GCMs: Ocean–atmosphere feedback analysis, *J. Clim.*, *20*, 4497–4525, doi:10.1175/JCLI4272.1.

Manganello, J. V., and B. Huang (2009), The influence of systematic errors in the Southeast Pacific on ENSO variability and prediction in a coupled GCM, *Clim. Dyn.*, *32*(7–8), 1015–1034, doi:10.1007/s00382-008-0407-5.

Mechoso, C. R., et al. (1995), The seasonal cycle over the tropical Pacific in coupled ocean–atmosphere general circulation models, *Mon. Weather Rev.*, *123*(9), 2825–2838, doi:10.1175/1520-0493(1995)123<2825:TSCOTT>2.0.CO;2.

Mechoso, C. R., et al. (2014), Ocean-cloud-atmosphere-land interactions in the southeastern Pacific: The VOCALS program, *Bull. Am. Meteorol. Soc.*, *95*, 357–375, doi:10.1175/BAMS-D-11-00246.1.

Meehl, G. A., C. Covey, T. Delworth, M. Latif, B. McAvaney, J. F. B. Mitchell, R. J. Stouffer, and K. E. Taylor (2007), The WCRP CMIP3 multimodel data set: A new era in climate change research, *Bull. Am. Meteorol. Soc.*, *88*, 1383–1394, doi:10.1175/BAMS-88-9-1383.

Rayner, N. A., D. E. Parker, E. B. Horton, C. K. Foll, L. V. Alex, D. P. Rowell, and A. Kaplan (2003), Global analyses of sea surface temperature, sea ice, and night marine air temperature since the late nineteenth century, *J. Geophys. Res.*, *108*(D14), 4407, doi:10.1029/2002JD002670.

Schneider, E. K. (2002), Understanding differences between the equatorial Pacific as simulated by two coupled GCMs, *J. Clim.*, *15*, 449–469, doi:10.1175/1520-0442(2002)015<0449:UDBTEP>2.0.CO;2.

Schneider, E. K., M. J. Fennessy, and J. L. I. Kinter (2009), A statistical-dynamical estimate of winter ENSO teleconnections in a future climate, *J. Clim.*, *22*, 6624–6638, doi:10.1175/2009JCLI3147.1.

Song, X. L., and G. J. Zhang (2009), Convection parameterization, tropical Pacific double ITCZ, and upper-ocean biases in the NCAR CCSM3. Part I: Climatology and atmospheric feedback, *J. Clim.*, *22*(16), 4299–4315, doi:10.1175/2009JCLI2642.1.

Szoeke, S. P. D., and S. P. Xie (2008), 2008: The tropical eastern Pacific seasonal cycle: Assessment of errors and mechanisms in IPCC AR4 coupled ocean–atmosphere general circulation models, *J. Clim.*, *21*, 2573–2590, doi:10.1175/2007JCLI1975.1.

Taylor, K. E. (2001), Summarizing multiple aspects of model performance in a single diagram, *J. Geophys. Res.*, *106*, 7183–7192, doi:10.1029/2000JD900719.

Taylor, K. E., R. J. Stouffer, and G. A. Meehl (2009), An overview of CMIP5 and the experiment design, *Bull. Am. Meteorol. Soc.*, *93*, 485–498, doi:10.1175/BAMS-D-11-00094.1.

Uppala, S. M., et al. (2005), The ERA-40 re analysis, *Q. J. R. Meteorol. Soc.*, *131*, 2961–3012, doi:10.1256/qj.04.176.

Yu, Y. Q., J. He, W. P. Zheng, and Y. H. Luan (2013), Annual cycle and interannual variability in the tropical pacific as simulated by three versions of fgoals, *Adv. Atmos. Sci.*, *30*(3), 621–637, doi:10.1007/s00376-013-2184-2.

Zhang, C. D. (2001), Double ITCZs, *J. Geophys. Res.*, *106*(D11), 11,785–11,792, doi:10.1029/2001JD900046.

Zhang, G. J., and H. Wang (2006), Toward mitigating the double ITCZ problem in NCAR CCSM3, *Geophys. Res. Lett.*, *33*, 272–288, doi:10.1029/2005GL025229.